Interplay of mulitphoton and tunneling ionization in short-wavelength-driven high-order harmonic generation

Vasileios-Marios Gkortsas,[1] Siddharth Bhardwaj,[1] Chien-Jen Lai,[1] Kyung-Han Hong,[1] Edilson L. Falcão-Filho,[2] and Franz X. Kärtner[1,3,*]

[1]*Department of Electrical Engineering and Computer Science and Research Laboratory of Electronics, Massachusetts Institute of Technology, Cambridge, Massachusetts 02139, USA*

[2]*Departamento de Física, Universidade Federal de Pernambuco, 50670-901, Recife, Pernambuco, Brazil*

[3]*DESY-Center for Free-Electron Laser Science and Hamburg University, 22607 Hamburg, Germany*

(Received 3 May 2011; published 29 July 2011)

High-order harmonic generation efficiency is theoretically modeled and compared with experiments using 400 and 800 nm driver pulses. It is shown that, for a short drive wavelength and a Keldysh parameter larger than 1, the Ammosov-Delone-Krainov (ADK) ionization model does not give a good agreement between theory and experiment. Since the ADK ionization model only accounts for tunnel ionization, it underestimates the yield of low-order harmonics from the wings of the driver pulse. In contrast, the Yudin-Ivanov ionization model [Phys. Rev. A **64**, 013409 (2001)], which accounts for both tunnel and multiphoton ionization, gives much better agreement with the experimental results.

DOI: 10.1103/PhysRevA.84.013427 PACS number(s): 32.80.Rm, 42.65.Ky

I. INTRODUCTION

High-order harmonic generation (HHG) driven by ultrashort laser pulses is widely used as a source for extreme ultraviolet (EUV) and soft-x-ray radiation because of its superb coherence properties in space and time as well as the compactness of the source. HHG can be described as a three-step process, which includes ionization, electron propagation, and recombination [1–3]. HHG has many applications in nanoscience, biology, and chemistry, however, it suffers from low conversion efficiencies. Since Ti : sapphire lasers became a standard high-power femtosecond laser source, most HHG experiments have been performed at its emission wavelength of 800 nm [4,5]. Typical conversion efficiencies from Ti : sapphire lasers are in the range of 10^{-6} to 10^{-8} for 50–100 eV photon energies. Many applications in the <100 eV range, such as EUV lithography, seeding of x-ray free-electron lasers, and attosecond spectroscopy require high energies or average power and, therefore, HHG needs higher efficiencies. For these applications the use of shorter driving wavelengths with slightly higher electric fields than that of 800 nm pulses is a favorable route towards higher HHG efficiencies because of the scaling of the single-atom response with drive wavelength and the reduced plasma dispersion, as discussed below.

In this paper, we compare the experimental results of HHG efficiency measurement using 400 and 800 nm driver pulses on several noble gases, as reported in [6], with a recently formulated theory [7,8].The driving wavelengths used are 400 and 800 nm and the targets are noble gases. We find that, for short drive wavelengths, the commonly used Ammosov-Delone-Krainov (ADK) ionization model [9] does not correctly predict the efficiencies for low-order harmonics. In contrast, the Yudin-Ivanov (YI) model [10] which takes both quasistatic tunneling and multiphoton ionization into account, leads to much better agreement between theory and experiment.

With the advent of new light sources like optical parametric amplifiers (OPAs) that allow different driving wavelengths for HHG, the scaling of the single-atom response versus drive wavelength has been extensively studied, showing that HHG efficiencies scale as λ^{-5} for the cutoff region and λ^{-6} for the plateau [8,11,12] for a fixed high-order harmonic wavelength. This scaling is due to quantum diffusion, energy scaling of a pulse with a fixed number of ionization cycles, and scaling of the frequency interval of a harmonic. In the case of the plateau region another factor λ^{-1} arises due to the quantum chirp.

According to the three-step model (TSM), the cutoff energy E_{cutoff} is given by the following formula [3]:

$$E_{\text{cutoff}} = I_p + 3.17\frac{E_0^2 e^2}{4m\omega_0^2}, \tag{1}$$

where I_p is the ionization potential, e and m are the electron charge and mass, respectively, and E_0 and ω_0 are the driver field amplitude and frequency, respectively. The cutoff energy of HHG driven by 800 nm pulses is typically in the range between 100 and 150 eV in He and below 100 eV in other noble gases. However, the efficiency is limited to below 10^{-7}, as mentioned above. On the other hand, for efficient harmonic generation in the energy range of 30–100 eV, the use of a 400 nm driver pulse, which is easily generated from frequency doubling of an 800 nm driver, is very promising due to the favorable wavelength scaling of the single-atom response. The desired EUV cutoff energy of the 800 nm driver can be achieved with a 400 nm driver by using slightly higher electric fields. In general, using the shortest wavelength possible to reach a given harmonic while being able to maintain phase matching leads to the highest possible efficiency. Short drive wavelengths are also appealing because the plasma contribution to phase matching is smaller than for long wavelengths and, as a result, the neutral contribution can be balanced by a higher ionization level. In other words, increasing the drive frequencies improves both the single-atom response due to reduced quantum diffusion and the phase

*kaertner@mit.edu

matching due to reduced plasma dispersion. This results in high overall efficiency.

II. THEORY OF HHG EFFICIENCY SCALING AND COMPARISON WITH EXPERIMENTS

To quantitatively confirm the experimental results presented in [6] we used the semi-analytic theory presented in [7] to calculate the efficiency for a single harmonic. Our model is one dimensional, uses the three-step model for calculation of the single-atom response in the single-active-electron approximation (SAE), and takes material properties and macroscopic effects into account.

The conversion efficiency into a given harmonic of ω_0, whose frequency is denoted by Ω, is given by

$$\eta = \frac{\int_{\Omega-\omega_0}^{\Omega+\omega_0} |\tilde{E}_h(\omega)|^2 d\omega}{\int_0^{\infty} |\tilde{E}(\omega)|^2 d\omega}, \tag{2}$$

where $\tilde{E}(\omega) \equiv \frac{1}{\sqrt{2\pi}} \int_0^T E(t) e^{i\omega t} dt$ is the Fourier transform of the driving field. Starting from the one-dimensional wave equation, we express the harmonic field $\tilde{E}_h(\omega)$ in terms of the dipole moment acceleration $\ddot{\xi}(t)$:

$$\tilde{E}_h(\omega) = -\frac{4\pi\alpha}{\sqrt{2\pi} i\omega\sigma(\omega)} g(\Delta k, L) \int_0^T \ddot{\xi}(t) e^{i\omega t} dt, \tag{3}$$

where $g(\Delta k, L) = [e^{i(\Delta k L)} - e^{-L/(2L_{\rm abs})}] / [1 + 2i(\Delta k L_{\rm abs})]$ is the macroscopic response for a phase mismatch Δk, L and $L_{\rm abs}$ are the interaction and absorption lengths respectively, α is the fine structure constant, and $\sigma(\omega)$ is the absorption cross section. The dipole moment acceleration is derived with the help of the Schrödinger equation in the strong-field approximation (SFA) using the Ehrenfest theorem [13] and is equal to

$$\ddot{\xi}(t) = 2^{3/2}\pi (2I_p)^{1/4} e^{i\pi/4} \times \sum_n \frac{a[t_{nb}(t)] a(t) \sqrt{w\{E[t_{nb}(t)]\}}}{E[t_{nb}(t)][t - t_{nb}(t)]^{3/2}} \alpha_{\rm rec} e^{-i\bar{S}_n(t)}, \tag{4}$$

where $w(E)$ is the ionization rate, $\alpha_{\rm rec} = \langle 0|V'(r)|\bar{p} - A(t)\rangle$ is the recombination amplitude calculated according to [14], $\bar{S}$ is the classical action, and t_b is the birth time of an electron that returns to the origin at time t. Assuming that the driving field is either a top-hat pulse of N cycles (sinusoidal with finite duration) or a Gaussian pulse with N cycles in the full width at half maximum (FWHM), we calculate the corresponding birth and arrival times of the trajectories (t_b,t) using equations of motion by assuming that the electrons are born with zero velocity.

We calculate the harmonic radiation and the efficiency for its generation by summing up the dipole acceleration occurring in each half-cycle of the field. We take into account the material properties and the ionization occurring within each half-cycle (dynamic ionization). Dynamic ionization and thus the corresponding dynamic phase mismatch are important for the quantitative agreement between theory and experiment.

The harmonic spectrum is given by

$$\begin{aligned}\tilde{E}_h(\omega) &= \frac{1}{\sqrt{2\pi}} \int_0^{2\pi(N-1)\omega_0} E_h(t) e^{-i\omega t} dt \\ &= -\frac{4\pi\alpha}{\sqrt{2\pi} i\omega\sigma(\omega)} \\ &\quad \times \sum_{n=0}^{N-2} \left(g(\Delta k_{2n+1}, L) \int_{\frac{2\pi}{\omega_0} n}^{\frac{2\pi}{\omega_0}(n+\frac{1}{2})} \ddot{\xi}(t) e^{-i\omega t} dt \right. \\ &\quad \left. + g(\Delta k_{2n+2}, L) \int_{\frac{2\pi}{\omega_0}(n+\frac{1}{2})}^{\frac{2\pi}{\omega_0}(n+1)} \ddot{\xi}(t) e^{-i\omega t} dt \right),\end{aligned} \tag{5}$$

where n denotes the full cycle and N is the total number of cycles [7]. The choice of the integration interval comes from the fact that high-order harmonics are only produced after the first three quarters of a cycle of the driver pulse and we neglect the last quarter of the last cycle for simplicity. Thus the integration is only over $N-1$ full cycles. The Fourier transform is carried out by using the periodicity of the driver pulse and trajectories in each half-cycle and factoring in the different half-cycle ionization levels. The expression accounts for the different phase mismatch Δk_n in each half-cycle. The ionization level during each half-cycle stays constant for the time interval where significant dipole radiation is generated and, as a result, the macroscopic response in each half-cycle is independent of time and can be taken out of the integral.

The expanded theory, including the dynamic ionization, is compared with our experimental results. Figure 1(a) shows the HHG efficiencies and spectra obtained experimentally using a 400 nm driver pulse for argon, neon, and helium, while Fig. 1(b) shows the corresponding simulation results. In the experiment, the peak intensity of the driver pulse measured from the peak power and spot size was 2.7×10^{15} W/cm^2 with

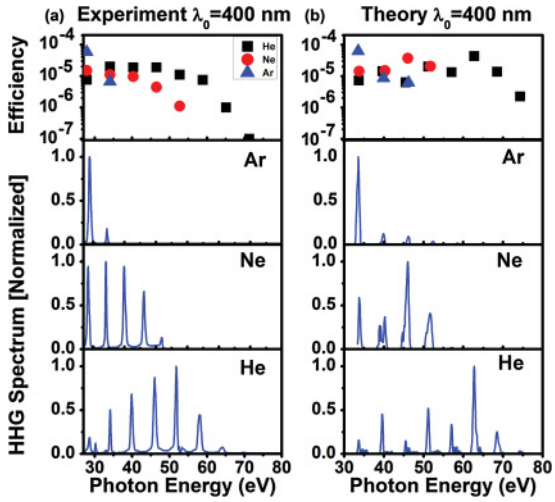

FIG. 1. (Color online) (a) Experimental results for HHG driven by 400 nm, 1 mJ, 26 fs driver pulses with 30 μm beam waist. Top row: efficiencies for Ar (50 mbar), Ne (300 mbar), and He (2 bar) using a 2-mm-long nozzle; remaining rows show the respective normalized HHG spectra [6]. (b) Simulation results for Ar (2.5×10^{14} W/cm^2), Ne (5.3×10^{14} W/cm^2), and He (8.5×10^{14} W/cm^2) for the same interaction parameters as in (a).

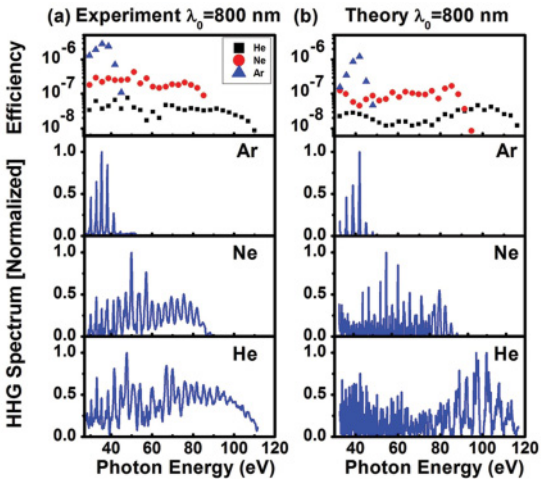

FIG. 2. (Color online) (a) Experimental results for HHG driven by 800 nm, 35 fs driver pulses with 40 μm beam waist. Top row: efficiencies for Ar (50 mbar, 0.6 mJ), Ne (300 mbar, 2 mJ), and He (2 bar, 2mJ) using a 2-mm-long nozzle; remaining rows show the respective normalized HHG spectra [6]. (b) Simulation results for Ar (1.2×10^{14} W/cm^2), Ne (3.2×10^{14} W/cm^2), and He (7.4×10^{14} W/cm^2) for the same interaction parameters as in (a).

a pulse energy of 1 mJ, with which we observed the strongest HHG signal. However, our theory suggests that this intensity will lead to strong ionization, which will make it difficult to achieve phase matching for the EUV wavelength. Thus, the actual intensity is estimated to be in the range of 10^{14}–10^{15} W/cm^2 due to spatial effects distorting the beam, such as plasma defocusing, which are not taken into account in the one-dimensional model. Actual measurements at intensities of about 10^{14} W/cm^2 show similar HHG efficiencies, as discussed in [6]. Therefore, in our simulations based on the one-dimensional model, we adjusted the laser intensity to achieve optimum phase matching conditions for the half-cycle in the center of the pulse. The intensities used in our simulations are lower than in the experiment. In the experiment, peak efficiencies of 1×10^{-4} at 28 eV are reached for Ar, 1×10^{-5} at 34 eV for Ne, and 1×10^{-5} at 53 eV for He, while the peak efficiencies from simulations are 6×10^{-5} at 33.5 eV for Ar, 2×10^{-5} at 51.7 eV for Ne, and 4×10^{-5} at 66.5 eV for He, which are close to the experiments. Figures 2(a) and 2(b) summarize the experimental and simulation results, respectively, for 800 nm drivers. As predicted by the theory, the efficiencies from the 800 nm driver are 1–2 orders of magnitude lower than that from the 400 nm driver. However, the cutoff energy is significantly increased to beyond 100 eV with He. In the experiment, the conversion efficiencies at the cutoff are 1×10^{-7} at 45 eV for Ar, 1×10^{-7} at 88 eV for Ne, and 1×10^{-8} at 110 eV for He, while the theory predicts 1×10^{-6} at 41 eV for Ar, 1×10^{-7} at 82 eV for Ne, and 1×10^{-8} at 107 eV for He.

In our simulations, in Figs. 1(b) and 2(b), we observe, in addition to intercycle interference which leads to odd harmonics, intracycle interference patterns on each harmonic. We observe that (a) theoretical HHG spectra do not show clean harmonics like their experimental counterparts and (b) that theoretical HHG spectra exhibit an interference structure even

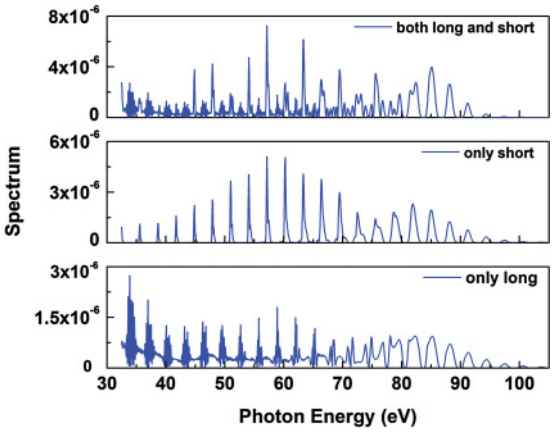

FIG. 3. (Color online) Theoretical power spectrum for neon at 800 nm when we keep (a) both short and long trajectories, (b) only short trajectories, and (c) only long trajectories.

within a harmonic. Both of the aforementioned discrepancies stem from the fact that, in the experiment, we collect mostly the radiation from short electron trajectories by optimizing phase-matching conditions and overall HHG yield, whereas in the theory the radiation from both the short and long electron trajectories is included in the harmonic spectrum. The intracycle harmonic structure is caused due to interference between the long and short trajectories which have the same return energy but different quantum phases [15]. Figure 3 shows the theoretical power spectrum for neon with 800 nm driver pulses when we keep both short and long trajectories [Fig. 3(a)], short trajectories only [Fig. 3(b)], and long trajectories only [Fig. 3(c)]. When we collect only the short trajectories the HHG spectrum shows clean harmonics without any interference structure. On the other hand, when we collect only the long trajectories the harmonics are not clean anymore and there is interference structure resulting from intercycle interferences. These intercycle interferences are caused by the different quantum phases of long trajectories in each

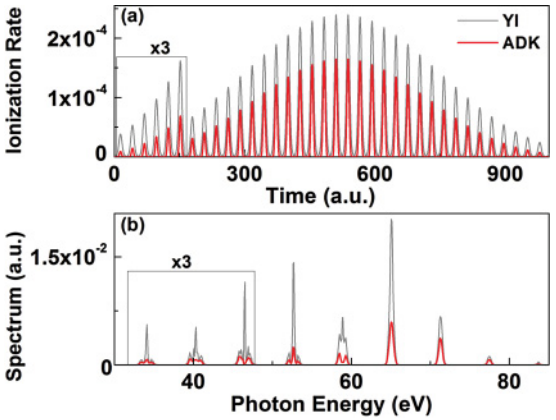

FIG. 4. (Color online) Ionization rates and spectral intensities of single-atom response in He for the same conditions as in Fig. 1 when using the YI (gray) and ADK [red (dark gray)] theory for 400 nm driver pulses ($\gamma \sim 1$). The insets show the ionization rates for the wings of the fields and the spectral intensities for the low-order harmonics pronounced three times.

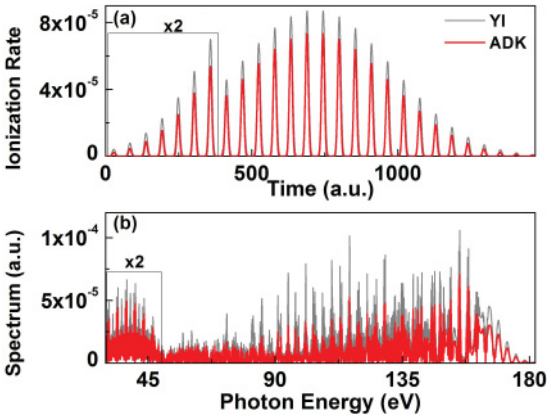

FIG. 5. (Color online) Ionization rates and spectral intensities of single-atom response in He for the same conditions as in Fig. 2 when using the YI (gray) and ADK [red (dark gray)] theory for 800 nm driver pulse ($\gamma \sim 0.52$). The insets show the ionization rates for the wings of the fields and the spectral intensities for the low-order harmonics pronounced two times.

half-cycle, which are strongly intensity dependent leading to incoherent addition of the different half-cycle contributions to the same harmonic. If the driver pulse is flat top, then the intensity would be identical in each half-cycle, the phases would add up coherently, and clear harmonics would appear.

III. COMPARISON OF IONIZATION MODELS

Ionization is the first step in the HHG process and the choice of the proper model to describe it is crucial in achieving good agreement between theoretical and experimental results. The most commonly used ionization model is the theory established by Ammosov, Delone, and Krainov, known as ADK theory. This model is preferred due to its computational convenience and is derived for the case of a dc driving field, which corresponds to $\gamma = 0$ and therefore the channel of ionization is pure tunneling. It is commonly used for sinusoidal driving fields but is valid only for a small Keldysh parameter

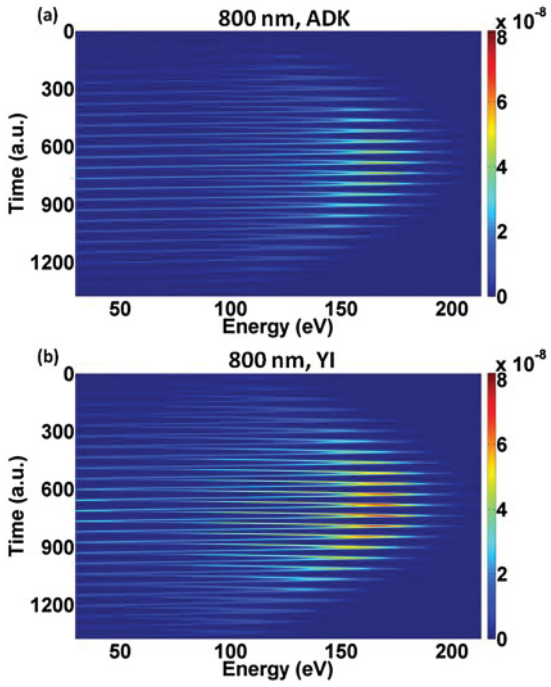

FIG. 6. (Color) Spectrogram of the HHG spectrum from 800 nm driver pulse using (a) ADK and (b) YI ionization rates, respectively. Both models (YI and ADK) predict similar low-frequency photon intensity in the wings of the driver pulse.

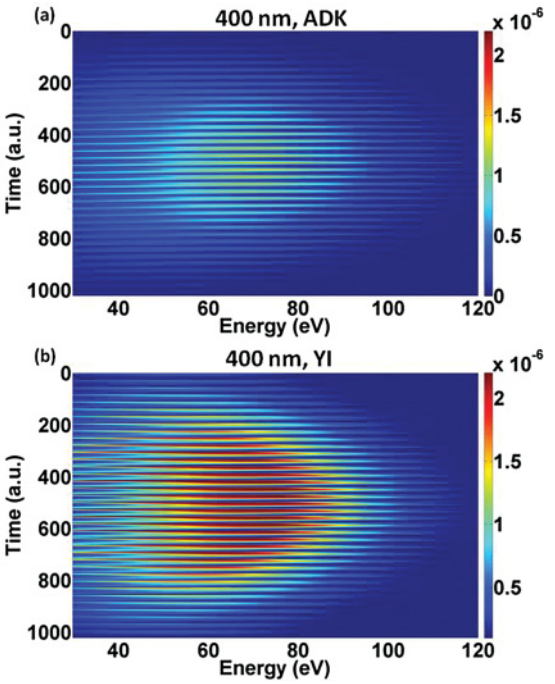

FIG. 7. (Color) Spectrogram of the HHG spectrum with 400 nm driver pulse using (a) ADK and (b) YI ionization rates, respectively. The YI model predicts a much higher low-frequency photon intensity in the wings of the driver pulse than does the ADK model.

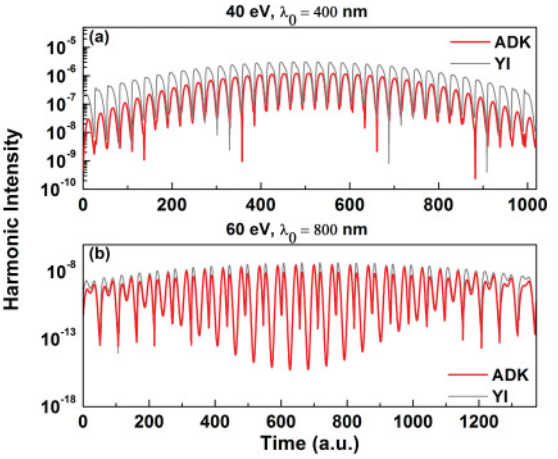

FIG. 8. (Color online) Harmonic intensity, calculated using YI and ADK theory for low photon energies. (a) For 40 eV and 400 nm driver pulses and (b) for 60 eV and 800 nm driver pulses. These ionization theories predict very different harmonic intensity, especially in the wings of the 400 nm driver pulse where γ is the largest.

for which the field-matter interaction is a nonperturbative process and tunneling is the main mechanism of ionization.

An alternative and more general method to calculate the ionization rate has been shown using the Landau-Dykhne method [10,16]. A detailed discussion of the Landau-Dykhne method can be found in [17–19]. This method is valid in the adiabatic regime and includes multiphoton and tunneling ionization and is referred to as Yudin-Ivanov (YI) ionization theory [10].

When using ADK theory for calculating the single-atom response, a mismatch between theoretical and experimental results is observed, especially for low-order harmonics by short driver wavelengths. The Keldysh parameter, which is inversely proportional to the electric field, is larger in the wings of the pulse than near the peak of the pulse. Additionally, by decreasing the wavelength of the driver pulse (from 800 nm to 400 nm), the Keldysh parameter becomes larger than 1 in the wings and multiphoton ionization becomes important. Hence, ADK theory cannot model the ionization process accurately as it underestimates the ionization yield. Therefore, we use YI ionization theory [in Figs. 1(b) and 2(b)] for calculation of the HHG spectra and we find that it results in much better agreement with experimental results than ADK theory.

To get more insight, we compare the ionization rates [Fig. 4(a) and 5(a)] and the single-atom response [Figs. 4(b) and 5(b)] calculated for a 400 and an 800 nm driver pulse using the ADK and YI ionization models, respectively. For a 400 nm Gaussian driver pulse with a peak intensity of 8.5×10^{14} W/cm^2 (Keldysh parameter $\gamma \sim 1$) the YI ionization rate is higher than the ADK rate over the entire pulse [Fig. 4(a)], but the relative mismatch is much more pronounced in the wings [Fig. 4(a), inset]. As a result, there is a noticeable difference between the HHG spectra generated by the two models, especially for low photon energies [Fig. 4(b), inset]. On the other hand, for 800 nm and a peak intensity 7.4×10^{14} W/cm^2 (Keldysh parameter $\gamma = 0.52$) the two models give similar ionization rates over the entire pulse [Figs. 5(a) and 5(a), inset]. The corresponding spectra generated from the two models are similar over the whole range of energies [Figs. 5(b) and Fig. 5(b), inset].

A time-frequency representation gives a better understanding of a dynamic process involving broad spectral components. For this purpose, we plotted the spectrograms of the high-order harmonic photons for 400 and 800 nm driver pulses using YI and ADK ionization models, as shown in Figs. 6–8. The spectrograms are calculated using a short-time Fourier transform with a Gaussian window function which has a FWHM of 58 attoseconds. In Fig. 6, we notice that the HHG spectrograms generated by the 800 nm pulse are insensitive to the choice of ionization model. However, this is not the case for the 400 nm driver pulse in Fig. 7. The spectrogram shows a higher photon yield over the different half-cycles of the driver pulse when we use the YI model of ionization. This contrast is further enhanced in the wings of the driver pulse where the Keldysh parameter is highest and multiphoton ionization is most prominent (Fig. 8). Since the ADK model underestimates the ionization rate in the wings of the 400 nm driver pulse, which contribute strongly to low-order harmonics, it drastically underestimates the low-order harmonic energy photon yield.

IV. CONCLUSIONS

In summary, we have compared our semi-analytic theory for calculating HHG efficiencies with experimental results for 400 and 800 nm driver pulses. We observed that using ADK ionization rates does not lead to a sufficiently good agreement between predicted and experimentally measured harmonic efficiencies, especially for low-order harmonics of the spectrum and a 400 nm driver pulse. Using the Yudin-Ivanov model, which includes multiphoton ionization, we predict the harmonic yield of low-order harmonics much more accurately. Our study shows that multiphoton ionization becomes as important or more important than tunneling ionization in the wings of the pulse, which significantly contribute to the low-order harmonics in the HHG process.

ACKNOWLEDGMENTS

The authors would like to thank Denys I. Bondar for helpful discussions. This work was supported by AFOSR Grants No, FA9550-09-1-0212 and No, FA9550-10-1-0063. V.-.M. Gkortsas acknowledges support from the Alexander S. Onassis Public Benefit Foundation and E. L. Falcão-Filho acknowledges support from the Conselho Nacional de Desenvolvimento Científico e Tecnológico, Brazil.

[1] K. C. Kulander, K. J. Schafer, and J. L. Krause, SILAP **316**, 95 (1993).
[2] P. B. Corkum, Phys. Rev. Lett. **71**, 1994 (1993).
[3] M. Lewenstein, P. Balcou, M. Y. Ivanov, A. L'Huillier, and P. B. Corkum, Phys. Rev. A **49**, 2117 (1994).
[4] E. A. Gibson, A. Paul, N. Wagner, R. Tobey, D. Gaudiosi, S. Backus, I. P. Christov, A. Aquila, E. M. Gullikson, D. T. Attwood, M. M. Murnane, and H. C. Kapteyn, Science **302**, 95 (2003).
[5] E. J. Takahashi, Y. Nabekawa, H. Mashiko, H. Hasegawa, A. Suda, and K. Midorikawa, IEEE J. Sel. Top. Quantum Electron. **10**, 1315 (2004).
[6] E. L. Falcão-Filho, C.-J. Lai, K.-H. Hong, V.-M. Gkortsas, S.-H. Huang, L. J. Chen, and F. X. Kärtner, Appl. Phys. Lett. **97**, 061107 (2010).
[7] V.-M. Gkortsas, S. Bhardwaj, E. L. Falcão-Filho, K.-H. Hong, A. Gordon, and F. X. Kärtner, J. Phys. B **44**, 045601 (2011).
[8] E. L. Falcão-Filho, V. M. Gkortsas, A. Gordon, and F. X. Kärtner, Opt. Express **17**, 11217 (2009).
[9] M. V. Ammosov, N. B. Delone, and V. P. Krainov, Sov. Phys. JETP **64**, 1191 (1986).
[10] G. L. Yudin and M. Y. Ivanov, Phys. Rev. A **64**, 013409 (2001).

[11] J. Tate, T. Auguste, H. G. Muller, P. Salières, P. Agostini, and L. F. DiMauro, Phys. Rev. Lett. **98**, 013901 (2007).
[12] A. D. Shiner, C. Trallero-Herrero, N. Kajumba, H.-C. Bandulet, D. Comtois, F. Legare, M. Giguere, J.-C. Kieffer, P. B. Corkum, and D. M. Villeneuve, Phys. Rev. Lett. **103**, 073902 (2009).
[13] A. Gordon and F.X. Kärtner, Phys. Rev. Lett. **95**, 223901 (2005).
[14] A. Gordon, R. Santra, and F.X. Kärtner, Phys. Rev. A **72**, 063411 (2005).
[15] G. Sansone, C. Vozzi, S. Stagira, and M. Nisoli, Phys. Rev. A **70**, 013411 (2004).
[16] D. Bondar, Phys. Rev. A **78**, 015405 (2008).
[17] J. P. Davis, J. Chem. Phys. **64**, 3129 (1976).
[18] A. M. Dykhne, Sov. Phys. JETP **14**, 941 (1962).
[19] A. V. Chaplik, Sov.Phys. JETP **18**, 1046 (1964).